Photodisintegration of ^{14}N: Cross Section and Angular Distribution for $^{14}N(\gamma, p_0)$*

R. W. Carr
Electron Accelerator Laboratory, Yale University, New Haven, Connecticut 06520
and
J. E. E. Baglin
Department of Physics, Iowa State University, and Ames Laboratory, U. S. Atomic Energy Commission, Ames, Iowa 50010
and
E. J. Bentz, Jr.
Niels Bohr Institute, Copenhagen, Denmark
(Received 6 April 1972)

The absolute cross section and angular distribution for the $^{14}N(\gamma, p_0)$ process have been measured, in the giant-resonance energy range from 17 to 25 MeV. Between 17 and 21 MeV, the large angular anisotropy requires mixing of at least two dominant $E1$ reaction channels. Above 22 MeV, d-wave emission from 2^- states appears to dominate. Admixture of about 5–10% of $E2$ and/or $M1$ strength is observed at all energies. The observations are qualitatively consistent with the shell-model predictions of Cooper and Eisenberg.

INTRODUCTION

The particle-hole shell-model description has been applied with some success to the photodisintegration of ^{16}O.[1,2] Recent experimental studies[3-7] of (γ, p) and (γ, n) channels in the giant resonance of ^{16}O have reached a degree of dependability and detail with which the theory can be examined rather stringently. In the ^{16}O case, evidence from (γ, p_0) and (γ, n_0) angular distributions[3] and (γ, n_0) polarization measurements[4] supports the basic idea that most of the giant-resonance strength derives from the excitation of a single particle from the $p_{3/2}$ state to the s-d shell with subsequent s- or d-wave emission. The principal structures in the ^{16}O cross section at 22 and 24 MeV have been attributed to $p_{3/2} \rightarrow d_{5/2}$ and $p_{3/2} \rightarrow d_{3/2}$ promotions, respectively.[3]

As a vehicle for testing the theoretical description, the ^{16}O photodisintegration has been shown to suffer from many complicating features whose full understanding and analysis will not be easy. For example, the initial ground-state configuration of ^{16}O is not pure $(p_{3/2})^8(p_{1/2})^4$ but it contains appreciable $(p)^{10}(2s, 1d)^2$ components[8] which need to be taken into account. It is also clear that appreciable influence on the cross sections is exerted by a 5–10% $E2$ or $M1$ component which interferes with the $E1$ components which we wish to study at all parts of the giant resonance.[3] At the present stage, considerations such as these have slowed progress in producing experimental results which can be expected to apply directly to the description given by existing simple theory.

The complications of surrounding conditions which tend to obscure any simple single-particle process are certain to be present in the case of ^{14}N also. However, the candidate dominant single-particle $E1$ promotions in ^{14}N remain the same as those in ^{16}O, namely $p_{3/2} \rightarrow (2s, 1d)$. In order to learn more about these transition processes set in a different nuclear environment, we have begun a study of giant-resonance reaction channels in ^{14}N.

The present paper reports cross section and angular distribution measurements for the (γ, p_0) process. These lead to conclusions about the multipole impurities in the ^{14}N case, and about the likely energy dependence of the dominant channels in this process.

Other work[9-11] covering the many other decay modes of the ^{14}N giant-resonance states, shows a great variety in the selective modes of decay. Combined with data on individual processes such as the present work, these results promise to be very informative regarding the basic dipole absorption process.

EXPERIMENTAL TECHNIQUE

The equipment and experimental procedures used have been described previously in detail.[3,12] Seven cooled 2-mm Si(Li) detectors were arranged to view a nitrogen gas target, at angles to the x-ray beam of 20, 45, 65, 90, 115, 135, and 160°. The apparatus and layout are shown schematically in Fig. 1.

Each detector was shielded from room background radiation by at least 20 cm of lead in all directions.

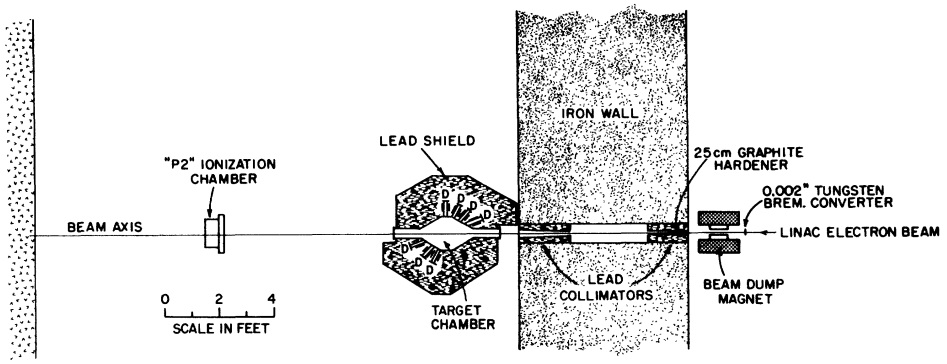

FIG. 1. Experimental geometry: $^{14}N(\gamma, p_0)$ angular-distribution study at Los Alamos electron prototype accelerator. A Si(Li) proton detector attached to a cold finger was located at each of the positions marked D.

Extensive precautions were required to minimize the background flux of beam-produced electrons which reach the detectors, causing undesirable background pulses. Pileup of these and foreground pulses was eliminated by the use of the 6% duty factor beam of the Los Alamos electron prototype accelerator (EPA), whose electron current on target was maintained typically at a stable 3 mA during the 450-μsec beam pulse. Permanent magnetic fields of 1.6 kG along a 15-cm portion of each detector access channel were designed to deflect all but the most energetic (>15-MeV) secondary electrons produced in the target, deflected electrons being stopped in a system of baffles.

Background runs with an evacuated target volume gave negligible yield. The effect of background energetic electrons and neutrons was measured by using the normal gas target but inserting 2-mm aluminum plates in the detector channels. These would stop all foreground protons but have little effect on energetic electrons and neutrons. Small count rates were observed up to pulse heights corresponding to about 5 MeV, and appropriate background subtractions were made.

The N_2 gas target was maintained at a pressure of 30 cm Hg, the pressure being dictated by the allowed resolution broadening for the 20 and 160° detectors caused by the finite target thickness traversed by the photoprotons. The target in this case was defined by the cylindrical profile of the collimated x-ray beam, whose diameter was 4.7 cm.

The geometrical efficiency of each detector was determined with an estimated over-all uncertainty of 2%. This efficiency is calculable using the expressions derived by Silverstein.[13] Its precision depends upon exact knowledge of the target chamber dimensions, detector sensitive area, and beam diameter and location. Annular masks close to the detector surfaces defined fully sensitive central areas of the detectors. Beam dimensions were verified by photographs fore and aft of the target chamber. Resulting computed efficiencies showed excellent agreement with measurements subsequently made using a standardized ^{241}Am α source.

The bremsstrahlung source was a 0.005-cm tungsten foil, receiving a beam of electrons whose energy spread was less than 1%. Transmitted electrons were swept out of the x-ray beam

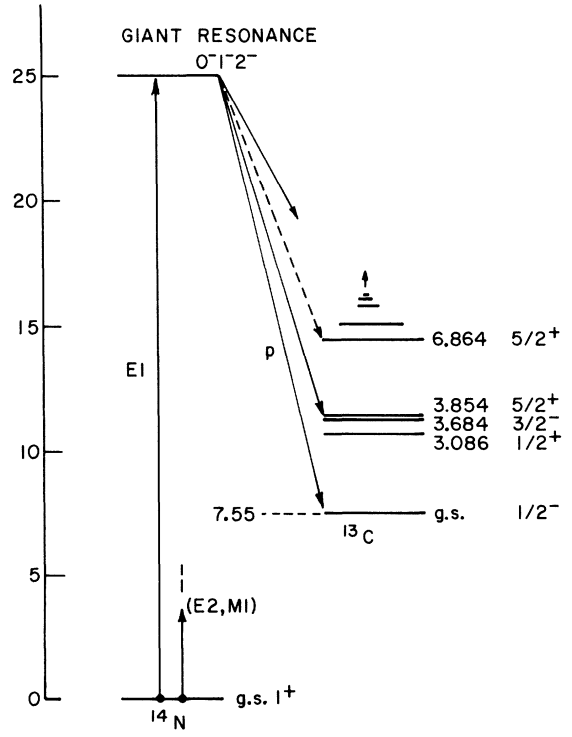

FIG. 2. $^{14}N(\gamma, p)^{13}C$ schematic level diagram (MeV units).

before it passed to a collimating system of length 2 m. A 25-cm graphite beam hardener was used.

A "P2" standard National Bureau of Standards specified[14] ionization chamber receiving the entire transmitted x-ray beam and feeding a current integrator was used to standardize absolute flux of thin-target bremsstrahlung. (Special auxiliary tests on this system confirmed within 1% the absence of any saturation effects at pulsed beam intensities ten times larger than those of the present experiment.)

Photoproton spectra were recorded using a multiplexing system and a single analog-to-digital converter, and were stored in a small on-line computer. Energy calibration of these spectra was based on trial spectra of ^{16}O photoprotons, in which the peaks at 22.10 and 24.15 MeV are readily identified. Assignment of these peak energies in the (γ, n) spectra[15,16] has been based with precision on well-known neutron absorption lines in ^{12}C.

The results presented here were fully confirmed

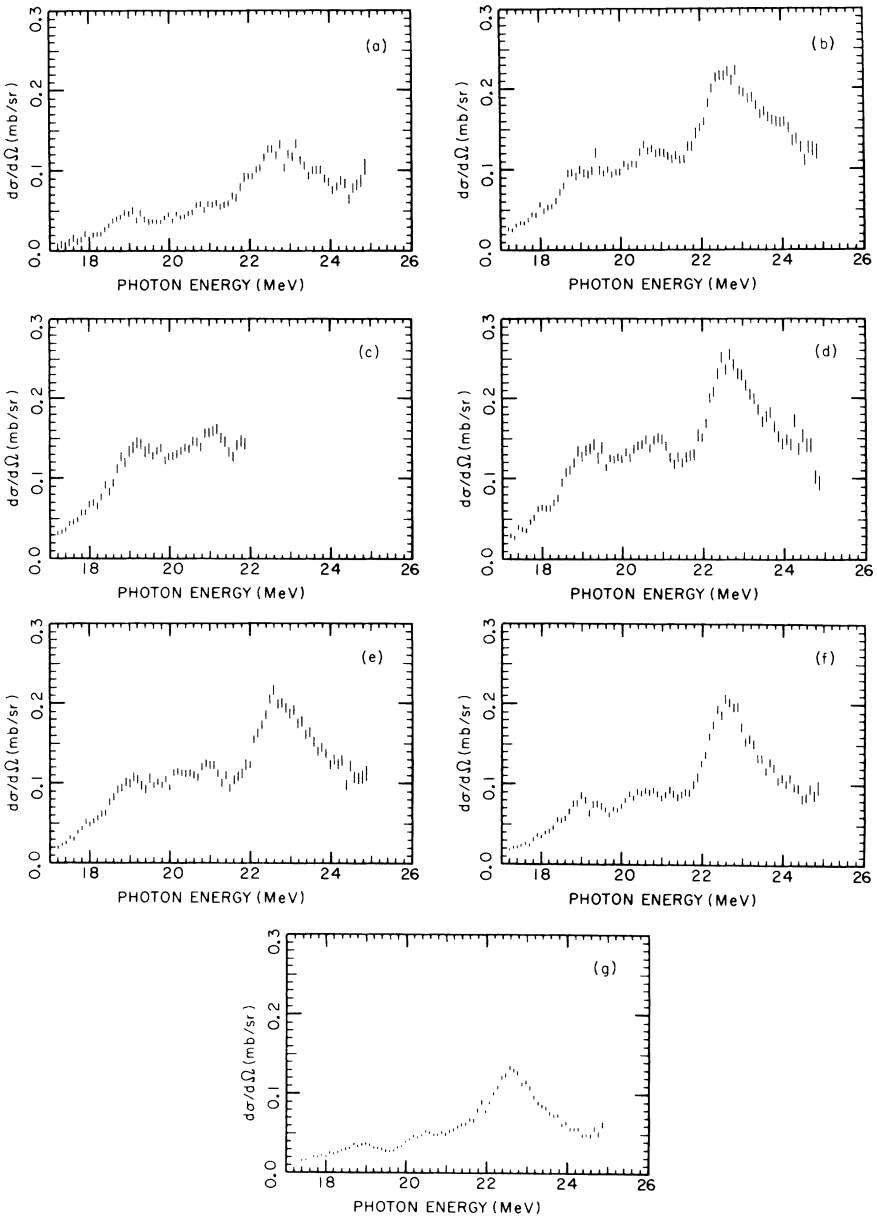

FIG. 3. $^{14}N(\gamma, p_0)$ differential cross section: (a) $\theta = 20°$; (b) $\theta = 45°$; (c) $\theta = 65°$; (d) $\theta = 90°$; (e) $\theta = 115°$; (f) $\theta = 135°$; (g) $\theta = 160°$.

in an independent set of runs six months later. Those runs used identical techniques in the course of a (γ, p_2) study on ^{14}N.

TREATMENT OF DATA

Photoproton spectra were taken with bremstrahlung end-point energies of 25.0, 22.5, and 20.5 MeV. Of each proton spectrum the highest 3-MeV energy region must originate with (γ, p) processes leading to the ground state of ^{13}C (see Fig. 2). Hence only that portion of each spectrum was used in this analysis. Being statistically poor and having a bremsstrahlung weighting sensitive to cutoff energy and spectral tip shape, the highest 0.5-MeV region of each spectrum was discarded.

From the remaining data, the weighting of the Schiff thin-target bremsstrahlung expression[17] was divided out, and a set of differential cross section results were obtained, in 100-keV intervals. Consistency checks were made by comparing successive runs having substantial energy overlap.

The over-all uncertainty assessed in the absolute cross-section scale is about 7%. Principal contributing uncertainties are: (i) 2–3% in absolute calibration of the "P2" beam monitor; (ii) 1% in target gas pressure monitoring; (iii) 2% in effective beam area; and (iv) approximately 2% in the geometrical efficiency of each detector. A smaller uncertainty applies to relative cross sections from one angle to another, which are needed to describe the angular distribution.

RESULTS

The ^{14}N(γ, p_0) differential cross sections obtained at six angles are shown in Fig. 3. Error bars shown are statistical standard deviations.

At each of the excitation energies shown (100 keV apart), the angular distribution was least-squares-fitted to a Legendre polynomial series of the form

$$\sigma(\theta) = A_0 + A_1 P_1(\cos\theta) + A_2 P_2(\cos\theta) + A_3 P_3(\cos\theta) + A_4 P_4(\cos\theta) . \quad (1)$$

The resulting coefficients are plotted, with their statistical uncertainties, as functions of excitation energy in Figs. 4 and 5. Their ratios to A_0 appear in Figs. 4 and 6.

The integral cross section from 18 up to 25 MeV

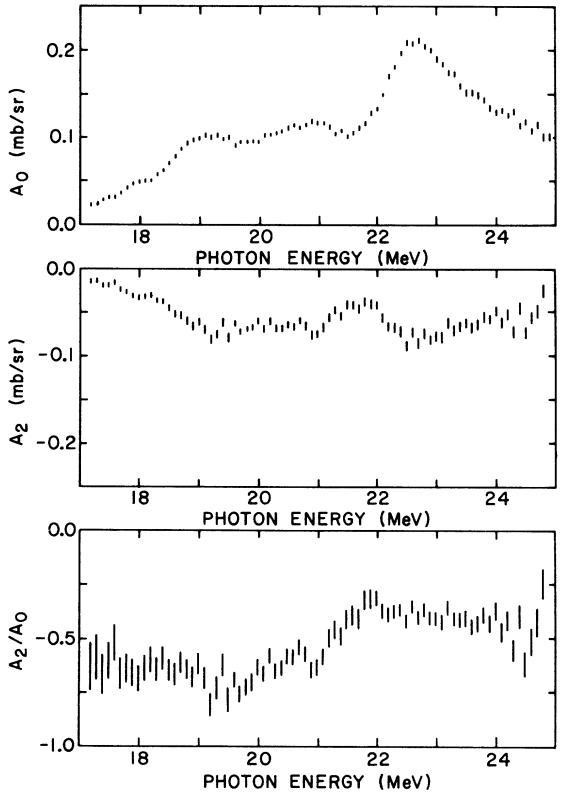

FIG. 4. ^{14}N(γ, p_0). Angular-distribution coefficients $A_0(=\sigma/4\pi)$, A_2, and the ratio A_2/A_0, plotted as functions of excitation energy in ^{14}N.

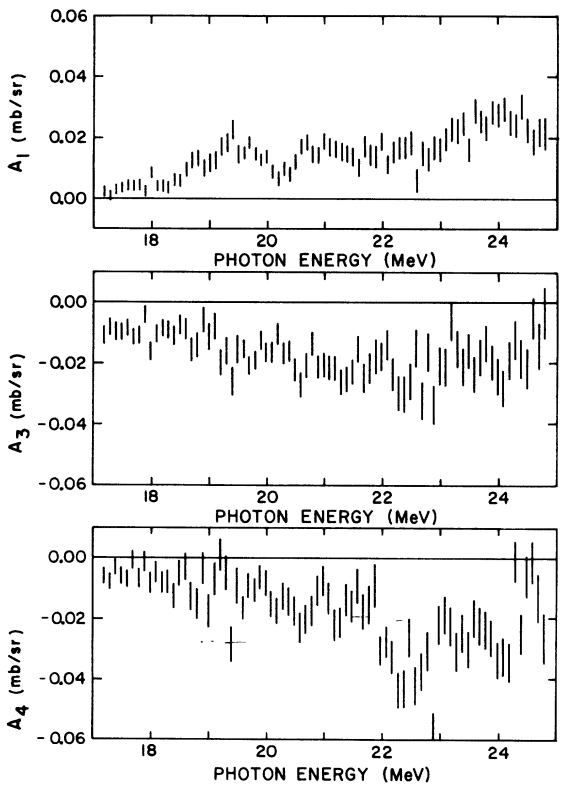

FIG. 5. ^{14}N(γ, p_0). Angular-distribution coefficients A_1, A_3, and A_4, plotted as functions of excitation energy in ^{14}N.

deduced from the present results is (11 ± 1) MeV mb. This represents only a small fraction (~10%) of the total absorption cross section to be inferred from the $[(\gamma, n) + (\gamma, np) + (\gamma, pn)]$ measurement by Berman *et al.*[11]

Figure 7 shows a comparison of the present 90° differential cross-section data with results obtained for $^{13}C(p, \gamma_0)$ by O'Connell[6] and for (γ, n_0) by Sherman *et al.*[10] The (γ, p_0) and (γ, n_0) cross sections appear to be effectively the same in magnitude and general shape. However, small disparities in structure appear to be real. Resolution differences may adequately account for discrepancies between (p, γ_0) data and the present work. The dramatic structure displayed in the (γ, p_0) results of Kosiek, Maier, and Schlupman[18] has not been substantiated.

DISCUSSION

The gross shape of the (γ, p_0) cross section (A_0) closely resembles that of the total photoneutron cross section[11] or that of the total photon-absorption cross section[19] up to 22.5 MeV. However, there appear to be resonance components in the 23- to 25-MeV region whose decay must favor residual states other than the ground state, since they are relatively weaker in the (γ, p_0) data.

The predictions of Cooper and Eisenberg[20,21] using a single-particle shell-model basis to compute energies and strengths of $E1$ photon absorption are shown in Fig. 8, overlaid with both (γ, p_0) and total absorption curves. In general terms, the computed distribution of $E1$ strength seems to match the total absorption curve. The higher-lying ^{14}N excited states evidently branch preferentially to excited residual states of ^{13}C.

Angular Distribution

Since the ^{14}N ground state has $J^\pi = 1^+$, an $E1$ excitation can produce a state of $J^\pi = 0^-$, 1^-, or 2^-. We use the channel-spin formalism to describe the angular distribution of photoprotons leaving ^{13}C in its ground $(\frac{1}{2}^-)$ state, following $E1$, $E2$, or $M1$ excitation of ^{14}N. Interference between all possible channels of identical channel spin is considered.

We denote by $(^E_M L, ljs)$ the matrix element associated with an electric (or magnetic) L-pole excitation of ^{14}N to a state of spin j which decays by emitting a proton of orbital angular momentum l with a channel spin s describing the decay channel. This notation accords with that of Carr and Baglin.[22] We may then write

$$(24/\lambda_\gamma^2) \cdot \frac{d\sigma}{d\Omega}(\theta) = \alpha_0 + \alpha_1 P_1(\cos\theta) + \alpha_2 P_2(\cos\theta) + \alpha_3 P_3(\cos\theta) + \alpha_4 P_4(\cos\theta), \quad (2)$$

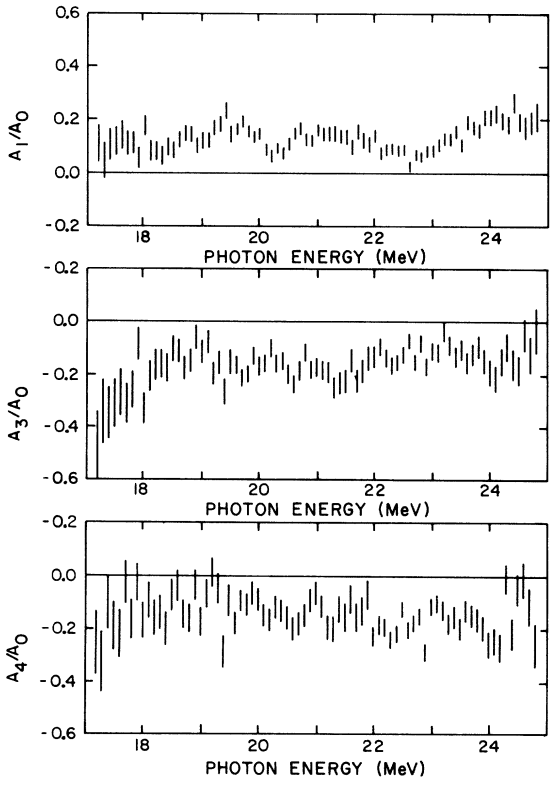

FIG. 6. $^{14}N(\gamma, p_0)$. Ratios of angular-distribution coefficients to A_0: A_1/A_0, A_3/A_0, and A_4/A_0, plotted as functions of excitation energy in ^{14}N.

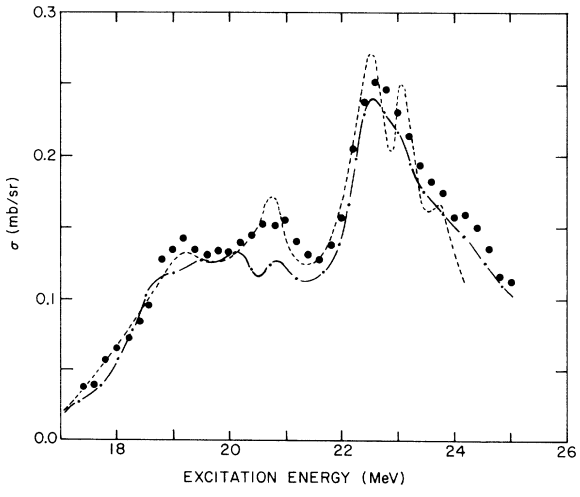

FIG. 7. $^{14}N(\gamma, p_0)$ differential cross section at 90°. Solid dots: present experiment. Dotted line: (p, γ_0) data (Ref. 6). Dashed line: (γ, n_0) data (Ref. 10).

where

$$\alpha_v = \sum_{uv} C_{t_u t_v v} \operatorname{Re}\{(^{E}_{M}L, ljs)^*_u\,(^{E}_{M}L, ljs)_v\}$$

with $t_u t_v$ referring to all parameters of channels u and v.

The coefficients C are fully tabulated in Ref. 22 for the case of interfering $E1$, $M1$, and $E2$ reaction channels. $E1$ contributions can be expected to dominate the even coefficients α_0 and α_2; α_1 and α_3 will carry evidence about the strength of the other interfering multipoles; α_4 involves only products of $E2$ terms.

A_0, A_2

To simplify first-order analysis, we neglect all but $E1$ terms in α_0 and α_2. The relevant $E1$ coefficients C are listed in Table I. Dropping the $E1$ prefix, the expressions for α_0 and α_2 thus become:

$$\alpha_0 = (000)^2 + 3(011)^2 + 3(211)^2 + 5(220)^2 + 5(221)^2,$$

$$\alpha_2 = 0.75(211)^2 - 2.50(220)^2 - 1.25(221)^2 + \operatorname{Re}\{3.16(000)^*(220) - 2.12(011)^*(211) - 4.74(011)^*(221) - 3.35(211)^*(221)\}. \quad (3)$$

With five contributing channels having unknown amplitudes and relative phases, exact solution from the present data is impossible. Some inferences however may be made, based on the magnitude of the observed ratio $A_2/A_0 (= \alpha_2/\alpha_0)$.

This ratio (Fig. 4) appears to be fairly constant (~−0.65) at energies below 21 MeV, and its value changes to a constant −0.40 above 22 MeV. Presumably this indicates a differing character in interfering resonances in the two regions. The pure (220) channel would yield $A_2/A_0 = -0.5$, and a little admixture of another channel would readily produce the observed high-energy value of −0.4. It is much more difficult to find a combination of terms which is capable of producing the large value of $A_2/A_0 = -0.65$ observed at low energies. With favorable phases, this could be generated by the (000) and (220) channels interfering. This would be consistent with the dominant ordering of states predicted by Cooper and Eisenberg.[20,21]

In practice, a more complex admixture should be expected. In fact, we note that the values of A_4 observed imply the existence of $E2$ strength too large to neglect (as we have just done) in any exact treatment. The above interpretation must therefore be regarded as somewhat speculative.

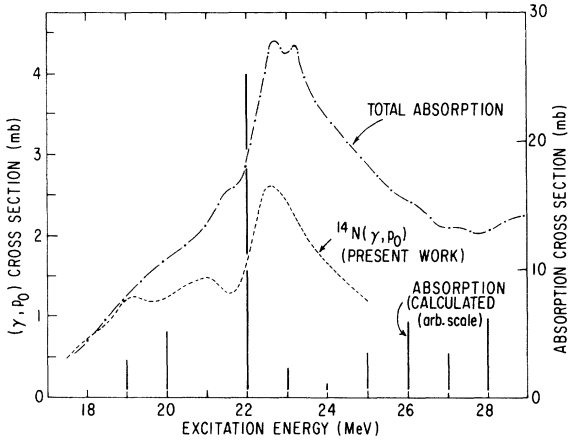

FIG. 8. Comparison of present results for ^{14}N(γ, p_0) cross section with total absorption cross-section data (Ref. 19) and one of the strength distributions calculated in Ref. 20 (Fig. 11).

TABLE I. Angular-distribution coefficients describing the $E1$ components of the reaction ^{14}N(γ, p_0). The notation used is that of Eq. (2) and of Ref. 22, from which the table is derived.

$E1(ljs)_u$	$E1(ljs)_v$	C_0	C_2
$E1$ 000	$E1$ 000	1.00	···
$E1$ 000	$E1$ 220	···	3.16
$E1$ 011	$E1$ 011	3.00	···
$E1$ 011	$E1$ 211	···	−2.12
$E1$ 011	$E1$ 221	···	−4.74
$E1$ 211	$E1$ 211	3.00	0.75
$E1$ 211	$E1$ 221	···	−3.35
$E1$ 220	$E1$ 220	5.00	−2.50
$E1$ 221	$E1$ 221	5.00	−1.25

A_1, A_3

These quantities consist entirely of interference terms between $E1$ and higher multipoles.

It is clear (Fig. 5) that at all energies both coefficients are very small, ($\leq 0.2\ A_0$). This implies a typical magnitude of the interfering amplitude around 5–10% of the $E1$ strength.

The nature of the $E2$ or $M1$ channels involved is not clear, owing to the large number of possible channels yet unidentified.

A_4

As seen in Figs. 5 and 6, A_4 is observed to be nonzero at most energies, with A_4/A_0 ranging from −0.1 to −0.2. A_4 arises entirely from terms which are products of $E2$ contributions, often being enhanced with large numerical coefficients. An $E2$ amplitude of about one-tenth the $E1$ amplitude could readily yield $A_4/A_0 = -0.2$, in accord with observation.

CONCLUSIONS

We find a 5–10% interfering $M1$ or $E2$ amplitude throughout the ^{14}N giant resonance as might be expected.

Further experimental work is required to provide more evidence on which to base identification of the dominant $E1$ channels and their energy dependence in the $^{14}N(\gamma, p_0)$ giant resonance. Measurements of photoneutron polarization would be of great value (as they have been in the case of ^{16}O).[4]

The present results are consistent with the distribution of $E1$ strength suggested by Cooper and Eisenberg,[21] in which interfering s- and d-wave channels dominate at lower energies, and d-wave channels alone account for the main giant resonance. More explicit study is needed. Significant insights might be expected from the study of ^{14}N decay modes to excited residual-state configurations.

ACKNOWLEDGMENTS

We wish to record our appreciation of the generous hospitality and encouragement of Dr. Louis Rosen, Dr. E. A. Knapp, J. Busick, and the staff of the Los Alamos Electron Prototype Accelerator.

---

*Work supported in part by the U. S. Atomic Energy Commission at Yale University and at the Ames Laboratory, Iowa State University.

[1]V. Gillet and N. Vinh Mau, Nucl. Phys. 54, 321 (1964).
[2]B. Buck and A. D. Hill, Nucl. Phys. A95, 271 (1967).
[3]J. E. E. Baglin and M. N. Thompson, Nucl. Phys. A138, 73 (1969).
[4]G. W. Cole, F. W. K. Firk, and T. W. Phillips, Phys. Letters 30B, 91 (1969).
[5]J. T. Caldwell, R. L. Bramblett, and S. C. Fultz, Phys. Rev. Letters 19, 447 (1967).
[6]F. Reiss, W. J. O'Connell, and P. Paul, Nucl. Phys. A175, 462 (1971).
[7]B. Ziegler, private communication.
[8]G. E. Brown and A. M. Green, Nucl. Phys. 75, 401 (1966).
[9]M. N. Thompson, R. J. J. Stewart, and J. E. M. Thomson, Phys. Letters 31B, 211 (1970).
[10]N. K. Sherman, R. W. Gellie, K. H. Lokan, and R. G. Johnson, Phys. Rev. Letters 25, 114 (1970).
[11]B. L. Berman, S. C. Fultz, J. T. Caldwell, M. A. Kelly, and S. S. Dietrich, Phys. Rev. C 2, 2318 (1970).
[12]J. E. E. Baglin and M. N. Thompson, Nucl. Instr. Methods 71, 71 (1969).
[13]E. A. Silverstein, Nucl. Instr. Methods 4, 53 (1959).
[14]J. S. Pruitt and S. R. Domen, National Bureau of Standards Monograph No. 48 (1962).
[15]F. W. K. Firk, *Annual Reviews of Nuclear Science* (Annual Reviews Inc., Palo Alto, California, 1970), Vol XX.
[16]C.-P. Wu, Ph.D. thesis, Yale University, 1969 (unpublished).
[17]H. W. Koch and J. W. Motz, Rev. Mod. Phys. 31, 920 (1959).
[18]R. Kosiek, K. Maier, and K. Schlupman, Phys. Letters 9, 260 (1964).
[19]N. Bezic, D. Brajnik, D. Jamnik, and G. Kernel, Nucl. Phys. A128, 426 (1969).
[20]B. S. Cooper and J. M. Eisenberg, Nucl. Phys. A114, 184 (1968).
[21]B. S. Cooper, Ph.D. thesis, University of Virginia, 1967 (unpublished).
[22]R. W. Carr and J. E. E. Baglin, Nucl. Data A10, 143 (1971).

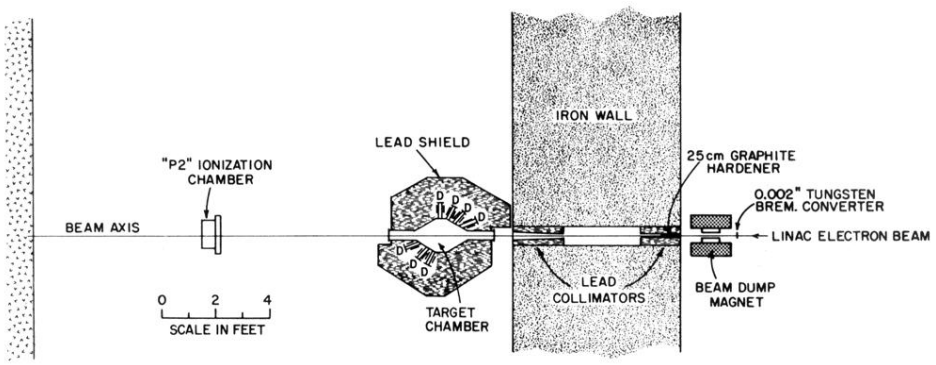

FIG. 1. Experimental geometry: $^{14}N(\gamma, p_0)$ angular-distribution study at Los Alamos electron prototype accelerator. A Si(Li) proton detector attached to a cold finger was located at each of the positions marked D.